HHS Public Access

Author manuscript

Mol Pharm. Author manuscript; available in PMC 2017 June 06.

Published in final edited form as:

Mol Pharm. 2016 June 06; 13(6): 1904–1914. doi:10.1021/acs.molpharmaceut.6b00069.

Hyaluronic Acid Molecular Weight Determines Lung Clearance and Biodistribution after Instillation

Christopher Kuehl[†], **Ti Zhang**[†], **Lisa M. Kaminskas**[‡], **Christopher J. H. Porter**[‡], **Neal M. Davies**[§], **Laird Forrest**[†], and **Cory Berkland**[†,∥,*]

[†]Department of Pharmaceutical Chemistry, The University of Kansas, Lawrence, Kansas 66047, United States

[∥]Department of Chemical and Petroleum Engineering, The University of Kansas, Lawrence, Kansas 66047, United States

[‡]Drug Delivery Disposition and Dynamics, Monash Institute of Pharmaceutical Sciences, Monash University, 381 Royal Parade, Parkville, Victoria, Australia, 3052

[§]College of Pharmacy, University of Manitoba, Winnipeg, Manitoba, Canada, R3E 0T5

Abstract

Hyaluronic acid (HA) has emerged as a versatile polymer for drug delivery. Multiple commercial products utilize HA, it can be obtained in a variety of molecular weights, and it offers chemical handles for cross-linkers, drugs, or imaging agents. Previous studies have investigated multiple administration routes, but the absorption, biodistribution, and pharmacokinetics of HA after delivery to the lung is relatively unknown. Here, pharmacokinetic parameters were investigated by delivering different molecular weights of HA (between 7 and 741 kDa) to the lungs of mice. HA was labeled with either a near-infrared dye or with iodine-125 conjugated to HA using a tyrosine linker. In initial studies, dye-labeled HA was instilled into the lungs and fluorescent images of organs were collected at 1, 8, and 24 h post administration. Data suggested longer lung persistence of higher molecular weight HA, but signal diminished for all molecular weights at 8 h. To better quantitate pharmacokinetic parameters, different molecular weights of iodine-125 labeled HA were instilled and organ radioactivity was determined after 1, 2, 4, 6, and 8 h. The data showed that, after instillation, the lungs contained the highest levels of HA, as expected, followed by the gastrointestinal tract. Smaller molecular weights of HA showed more rapid systemic distribution, while 67 and 215 kDa HA showed longer persistence in the lungs. Lung exposure appeared to be optimum in this size range due to the rapid absorption of <67 kDa HA and the poor lung penetration and mucociliary clearance of viscous solutions of HA > 215 kDa. The versatility of HA molecular weight and conjugation chemistries may, therefore, provide new opportunities to

[*]**Corresponding Author**, The University of Kansas, 2030 Becker Drive, Lawrence, KS 66047. Phone: (785) 864-1455. Fax: (785) 864-1454. berkland@ku.edu.

ASSOCIATED CONTENT

Supporting Information

The Supporting Information is available free of charge on the ACS Publications website at DOI: 10.1021/acs.molpharmaceut.6b00069.

Organ clearance rate for each tissue and exposure levels of HA in the lungs and the four extracted lymph nodes (PDF)

The authors declare no competing financial interest.

extend pulmonary drug exposure and potentially facilitate access to lymph nodes draining the pulmonary bed.

Graphical Abstract

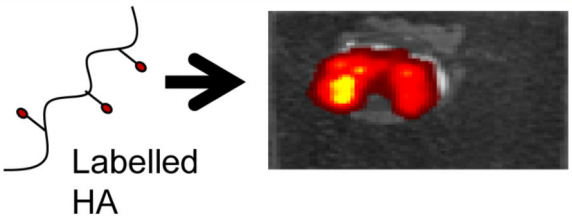

Keywords

haluronic acid; pulmonary delivery; biodistribution; pulmonary transport; radiolabeled; pharmacokinetics

1. INTRODUCTION

Hyaluronic acid (HA) is a linear biopolymer component of multiple approved products and exhibits versatility for drug delivery, since it is available in a wide range of molecular weights and offers multiple sites for chemical modification.[1–6] In the human body, HA is prevalent in cartilage, skin, and synovial fluid and is typically present as a very high molecular weight (up to 20 MDa) polymer, providing elasticity to tissues. As HA degrades, it drains away from these tissues, percolating with interstitial fluid into and through lymph nodes with a portion passing into the systemic circulation.[7–13] Thus, HA serves as an interesting polymer to carry drugs. Absorption of HA after subcutaneous,[14–18] intraperitoneal,[19] oral,[20,21] and intravenous injection[22–24] has been reported, but the fate of HA after pulmonary administration is not well understood. Recent work suggesting that HA may be useful for inhaled drug delivery motivates a better understanding of HA fate after pulmonary administration.[25–29]

The lungs eliminate materials using active transport processes including mucociliary and macrophage clearance, as well as passive diffusion to the bloodstream or lymph.[30] Mucociliary clearance occurs in the upper airways as ciliated cells sweep mucus up the trachea and into the oropharyngeal cavity where it is typically swallowed. HA residence time in the upper airways, therefore, depends on the distance from the site of deposition to the oropharyngeal cavity. The rate of mucociliary clearance can also depend on mucus viscosity. Slower and/or incomplete clearance of thick mucus is observed clinically while expectorants facilitate better mucus clearance. Further down the airways in the terminal bronchioles and alveoli, macrophages can recognize molecules or particles. Macrophages that have bound or phagocytosed HA can then actively traffic to the lymphatics draining the pulmonary bed. Finally, HA molecules may dissolve into the fluid layer lining the lung epithelium and then passively diffuse into the bloodstream.[30–33] This mode of systemic absorption is usually fastest in the alveolar region, where the tissue barriers are as thin as a few hundred nanometers.[32,34] Passive diffusion into the lymphatic network draining the

lungs may also be possible, although this clearance mechanism might be expected to be slower compared to absorption into the bloodstream.[30,32,33]

In general, endogenous HA present in tissues has several different elimination routes as it is degraded to lower molecular weight chains through enzymatic and nonenzymatic mechanisms.[7–13] Endogenous HA that is part of the extracellular matrix or synovial fluid is on the order of 4–20 MDa in size. Enzymatic reactions that degrade HA occur in the interstitial space, in lymph, or in the blood by enzymes such as hyaluronidase. Nonenzymatic degradation of HA can occur by nonspecific chemical reactions including acidic or alkaline hydrolysis or oxidation. These degradation pathways yield smaller HA fragments (hundreds of kDa in size), which then drain with interstitial fluid.[7–13]

The interstitial fluid is collected into the lymphatics, where the majority of HA fragments smaller than 450 kDa are removed from the lymph fluid during filtration through lymph nodes before the fluid is passed back into the blood.[35,36] These HA fragments are then further degraded into even smaller fragments in the lymph nodes since the majority of HA turnover occurs in the lymphatics, thereby eliminating the HA fragments before they enter the blood circulation.[6–8] Lymphatic drainage of HA can be facilitated by active transport by binding to CD44 expressed on the surface of macrophages or lymphocytes.[37,38] Some HA fragments can reach the systemic circulation from the interstitial fluid. In the blood, HA plasma clearance is rapid (half-life as low as 2 min).[22] Larger HA fragments (hundreds of kDa in size), circulate until reaching the liver, where endothelial cells remove HA from circulation.[5,39,40] Smaller molecular weight HA fragments are eliminated by the kidneys since molecular weight cutoff for efficient urinary excretion is approximately 25 kDa.[4,5,22]

The lungs offer a route of administration that can facilitate local therapy, access to the systemic circulation, and perhaps even delivery to pulmonary lymph nodes. HA is likely to be well-tolerated in the lungs as evidenced by studies where HA has been delivered by inhalation to dogs[41] or nebulized into humans to treat lung inflammation.[25–29] In addition, HA is emerging as an important carrier molecule for drug delivery. In the present study, HAs of discrete molecular weights were administered to the lungs of mice via intratracheal instillation to determine how HA molecular weight dictates persistence in the lung, systemic absorption, and access to lymph nodes draining the pulmonary bed. HA molecular weights of 7, 30, 67, 215, and 741 kDa were studied, and biodistribution was assessed by using fluorescent or radiolabeled HA.[3,42–44]

2. MATERIALS AND METHODS

2.1. Materials

The different molecular weights (7.5, 29/31, 67, 215, and 741 kDa) of hyaluronic acid (HA) were obtained from Lifecore Biomedical (Chaska, Minnesota). The 29/31 kDa HA (herein referred to as 30 kDa HA) was received in two different lots, with average molecular weights of 29 kDa and 31 kDa. The near-infrared dye, HiLyte Fluor 750 hydrazide, was obtained from AnaSpec (Fremont, California). DMTMM (4-(4,6-dimethoxy-1,3,5-triazin-2-yl)-4-methylmorpholinium chloride) was obtained from ChemPep Inc. (Wellington, Florida). Pierce iodination beads were purchased from Thermo Scientific (Rockport, Illinois)

and NaI^{125} from PerkinElmer (Waltham, Massachusetts). The mouse laryngoscope was obtained from Penn-Century (Wyndmoor, Pennsylvania). All water used was deionized (DI) water from a Labconco Pro PS system. All other chemicals and materials including tyrosine, EDC (1-ethyl-3-(3-(dimethylamino)propyl)carbodiimide), 3500, 20000, and 50000 Da molecular weight cutoff dialysis tubing, PD-10 columns, bent fine dissecting forceps, glacial acetic acid, sodium acetate, sodium phosphate monobasic monohydrate, sodium phosphate dibasic, Fisherbrand disposable culture tubes (12 × 75 mm), and phosphate buffered saline were purchased from Fisher Scientific (Pittsburgh, Pennsylvania).

2.2. Near Infrared Dye Labeling of HA

A 1 mg vial of HiLyte Fluor 750 hydrazide dye was dissolved in 1 mL of 50 mM acetate buffer, pH 5.0. HA (7.5 mg) was dissolved in 4 mL of 50 mM acetate buffer, pH 5.0, with 0.5 equiv of EDC to which the 1 mg/mL of dye was added.[2,44–49] The reaction was allowed to proceed for approximately 16 h at room temperature and and the mixture stirred at 450 rpm protected from light. After 16 h, the reaction mixture was dialyzed using 3500 Da molecular weight cutoff dialysis tubing for 7.5 kDa HA, 20000 Da molecular weight cutoff dialysis tubing for 30 kDa HA, and 50000 Da molecular weight cutoff dialysis tubing for 67, 215, and 741 kDa HA; the dialysate was replaced every 6 h for 24 h. The HA–IR dye conjugate was removed from the tubing and then frozen at −20 °C. Samples were lyophilized for 72 h at a temperature of −72 °C at a vacuum of <300 mTorr (VirTis Freezemobile-12XL, The VirTis Company, Gardiner, New York). Samples were reconstituted using DI water to a concentration of 1 mg/mL prior to instillation.

Conjugation of the dye to HA was confirmed using HPLC (Figure 1). The conjugation efficiency of the dye was determined by taking a sample of the reaction mixture and comparing the intensity of the fluorescent peak before and after dialysis. The HPLC–fluorescence system consisted of a Shimadzu CBM-20A system controller, a LC-20SB solvent delivery pump, a RF-10A XL Shimadzu fluorescent detector, and a SIL-20 AC HT autosampler (Shimadzu Corp, Kyoto, Japan). Chromatograms were acquired and analyzed using LC Solutions software. An isocratic system with a mobile phase of 50 mM acetic acid, pH 5.0, was used with a Vydac HPLC protein and peptide C18 column (5 μm particles, 4.6 mm × 250 mm). The flow rate was 0.5 mL/min, the injection volume was 20 μL, and the excitation and emission wavelengths were 753/782 nm, respectively. The HA samples were diluted to a concentration of approximately 1 mg/mL using the mobile phase and had a retention time of 20.75 min.

2.3. Radiolabeling of HA

For radiolabeling of HA, 60 mg of HA was dissolved in 3 mL of 1 mM phosphate buffer pH 6.0 with 13.5 mg of tyrosine (0.5 equiv). The pH was adjusted back to 6.0 using 1.0 M HCl, after which 20.7 mg of DMTMM was added (0.5 equiv). The reaction mixture was stirred at 175 rpm for approximately 16 h at room temperature. Afterward, samples were dialyzed, lyophilized, and reconstituted as necessary as described previously. [3,24,42–44,50–52]

Conjugation of tyrosine to HA was confirmed by 1D proton NMR. The NMR was run using a scan rate of 16 scans and 2 dummy scans using deuterium oxide as the solvent at a

concentration of 10 mg/mL. The NMR was a 400 MHz Bruker (Billerica, MA) AV spectrometer equipped with an X-channel observe probe. Conjugation efficiency was calculated by comparing the integration of HA peaks to the integration of tyrosine peaks. The conjugation efficiency of tyrosine to 741 kDa HA was unable to be determined due to viscosity issues limiting the concentration of the sample.

Iodine labeling was performed using iodination beads (Figure 1). Two iodination beads were used per HA molecular weight sample and were rinsed with 10× PBS for 3 min. The beads were then dried on filter paper, added to 200 μL of $Na^{125}I$ (1 mCi) in 10× PBS, and incubated for 5 min at room temperature. HA–tyrosine (150 μL of 1 mg/mL) was added to the $Na^{125}I$, and the bead solution was incubated overnight at room temperature. The reaction mixture was then transferred to an equilibrated PD-10 column. To elute the HA–^{125}I, 6 mL of PBS was added, and 500 μL fractions were collected in Eppendorf tubes. From each fraction, 10 μL was taken and transferred to a new Eppendorf tube and counted using a Canberra model 2000 NIM BIN with Canberra model 802-4W NaI Well (3″ by 3″ well) detector gamma counter. The amplifier was a Canberra model 814A with a Ortec model 775 counter, Ortec model 719 timer, Ortec model 495 power supply, and a Canberra model 2030 single channel analyzer (SCA). The settings used were an amplifier coarse gain of 8 and fine gain of 8.8 with the power supply set at 875, SCA of Delta E: 10 and a lower level discriminator of 0.06. To determine conjugation efficiency of ^{125}I to HA–tyrosine, an ethanol precipitation method was used. The highest intensity vial from the 10 μL aliquot of HA–tyrosine–^{125}I (from now on HA–^{125}I) PD-10 eluents had 20 μL of 20 mg/mL HA added followed by the addition of 200 μL of cold ethanol. The mixture was put on dry ice for 20 min and then was centrifuged at 2000 rpm for 20 min on a Biofuge A centrifuge by American Scientific Products. The supernatant was then separated from the pellet, and both were recounted on the scintillation counter. Equation 1 was used to determine the conjugation efficiency from the scintillation data. All radiolabeling was conducted under the supervision of the University of Kansas Radiation Safety Committee.

$$\text{conjugation efficiency} = \frac{\text{pellet radioact.(cpm)}}{\text{pellet radiaoct.(cpm)} + \text{supernatant radioact.(cpm)}} \times 100\% \quad (1)$$

To prepare the HA–^{125}I for intratracheal instillation, a similar ethanol precipitation procedure was used. Approximately 22–25 mg of HA was dissolved in 500 μL of water, and then a 500 μL fraction of HA–^{125}I collected from the PD-10 column was added. The HA–^{125}I/HA solution was precipitated with approximately 12 mL of cold ethanol, and after sitting on dry ice for 10 min, the sample was centrifuged for 10 min at 12000 rpm using a Dynac 2 centrifuge from Becton Dickinson. The supernatant was removed, and the pellet was dissolved in 2 mL of DI water (for HAs < 700 kDa) or 3 mL of DI water for the 741 kDa HA.

2.4. Sizing of HA

Size exclusion chromatography (SEC) was employed to determine the difference in molecular weight between HA and HA–tyrosine. Samples were analyzed at a concentration

of 5 mg/mL. The system used was a Waters e2695 separation module, Waters 2414 refractive index detector, and Waters 2489 UV/vis detector with two columns in series: a PL Aquagel-OH 60 Analytical SEC (300 × 7.5 mm) and then a PL Aquagel-OH 40 Analytical SEC (300 × 7.5 mm) (Santa Clara, California). Samples (80 μL of 5 mg/mL) were dissolved and run using an isocratic 0.5 mL/min mobile phase of 0.1 M ammonium acetate with 0.136 M sodium chloride at pH 5. Chromatograms were analyzed using EMPower 3.

Dynamic light scattering (DLS) of HA was executed to determine the approximate physical size of the HA in solution. DLS was performed using a ZetaPALS (Brookhaven Instruments Corp., ZetaPALS, Holtsville, New York). HA was dissolved in 1× PBS at a concentration of 1 mg/mL and filtered through a 0.45 μm filter. Measurements were performed in a glass cuvette using ZetaPALS software (Holtsville, New York).

2.5. Animals

BALB/C mice (female, 4 weeks old at 13–16 g) were supplied by Monash Animal Research Services (Victoria, Australia) for the near-infrared dye imaging and by Harlan Laboratories (Indianapolis, Indiana) for the radio-labeling. One group of Harlan mice was used in a crossover study of near-infrared dye imaging to confirm similar pharmacokinetic behavior between the different suppliers. Mice were maintained on a 12 h light/dark cycle and were fed standard rodent pellets with no dietary restrictions nor withheld food. Water was freely available at all times. All animal experiments were approved by the Monash Institute of Pharmaceutical Sciences or the University of Kansas Institutional Animal Care and Use Committee (IACUC).

2.6. Intratracheal Instillation of HA

For lung administration via intratracheal instillation, each animal was anesthetized with 2% isoflurane in an induction chamber for approximately 4 min. The unconscious mouse was positioned in dorsal recumbency using a dosing board at approximately 60° to a supine position suspended by incisor teeth using a thin wire. A nose cone was used to maintain anesthesia.[53] The mouth was opened and the tongue was gently pulled out and to the side of the mouth. A laryngoscope was then positioned to depress the tongue and visualize the vocal cords at the top of the trachea. A 50 μL solution of labeled HA was then pipetted at the top of the trachea. The tongue was withheld for at least 3 breaths, after which time the mouse was maintained under anesthesia for an additional 3 min on the dosing board. The mouse was then removed from the dosing board and allowed to recover from the anesthesia by being held vertically until movement was regained. For the near-infrared dye, 1 mg/mL of HA-IR dye was instilled, and for the radiolabeled HA, approximately 11–12 mg/mL HA for 7, 30, and 67 kDa HA, 2.8 mg/mL for 215 kDa HA, and 1.6 mg/mL for 741 kDa HA was instilled according to Table 1.

2.7. Near Infrared Dye Ex Vivo Imaging

At 1, 8, or 24 h after intratracheal instillation, mice were euthanized via an ip injection of sodium pentobarbital (>100 mg/kg body weight), and death was confirmed by the absence of a heartbeat. The lungs, trachea, heart, spleen, liver, kidney, stomach, intestine, and bladder were then excised to evaluate the relative distribution of HA in mice at the different time

points. Fluorescent images were collected on a Caliper Life Sciences IVIS Lumina II from Thermo Fisher Scientific (Victoria, Australia) using living image V 4.3.1 software from Caliper Life Sciences, Waltham, Massachusetts. A 745 nm wavelength bandpass filter was used for excitation and 780 nm as the emission filter. All points included at least 3 mice. Fluorescent images that were repeated and collected at the University of Kansas were performed on a Cambridge Research and Instrumentation Maestro multispectrum imager (Woburn, Massachusetts) with an excitation filter of 710–760 nm and long pass emission filter of 800–950 nm.

2.8. Counting of Signals from Radiolabeled Tissue

At 1, 2, 4, 6, and 8 h after intratracheal instillation, mice were euthanized via isoflurane overdose in an inhalation chamber in a hood, and death was confirmed by cessation of breathing for 5 min. The tissues of interest were then surgically removed including the right axillary and brachial lymph nodes, the left axillary and brachial lymph nodes, trachea, heart, right and left lung lobes, spleen, liver, stomach, intestine, kidneys, bladder, and final fecal pellet in the GI tract. Each tissue sample was suspended in approximately 2–3 mL of 1× PBS in 12 by 75 mm glass Fisherbrand tubes. Samples were scintillated on a Beckman Gamma 5500B system with a 3″ by 3″ NaI detector. Counts were taken for 1 min, and the average of 3 or more readings was used. All bladders were assayed without urine to keep the measurements consistent. Samples were corrected for dose and radiolabeling efficiencies. All time points for all test articles exhibited <5% error for the measurement except for the intestine 7 kDa HA at 1 h and 741 kDa at 1 and 2 h.

2.9. PK Analysis of Radiolabeled Tissue

Pharmacokinetic (PK) analysis of the radiolabeled HA data was performed using WinNonlin 6.3 software. Noncompartmental modeling analysis was performed assuming first order input with uniform weighting using extravascular dosing, plasma type model for tracking, and trapezoid linear interpolation to calculate PK parameters.

3. RESULTS

3.1. Size Characterization of HA

The selection of the molecular weights of HA (7, 30, 67, 215, and 741 kDa) provided a size range representative of endogenous median to low molecular weight HA with regular size intervals. Theoretical radii of gyration and theoretical hydrodynamic radii were calculated utilizing eq 2 and eq 3 respectively.[54,55] Theoretical radii of gyration ranged from 7 to 100 nm across the molecular weights of HA studied, and theoretical hydrodynamic radii ranged from 3 to 54 nm (Table 1).

$$\mathrm{Rg}=2.35[\mathrm{MW\ \ in\ \ kDa}]^{0.57} \quad (2)$$

$$\mathrm{Rh}=0.87[\mathrm{MW\ \ in\ \ kDa}]^{0.63} \quad (3)$$

DLS was performed on the different molecular weights of HA to compare the measured hydrodynamic radii of HA molecules to the calculated values. As expected, the measured size increased with molecular weight (Table 1). The size of HA increased from 6 to 55 nm, which corresponded relatively well to the theoretical estimates of the radius of gyration and hydrodynamic radius.

3.2. HA–Fluorescent Dye Conjugation Efficiency

In general, the conjugation efficiency of the IR hydrazine dye decreased with increasing molecular weight (Table 2). The smaller HA molecules (7 and 30 kDa) had similar conjugation efficiencies that were nearly double the conjugation efficiencies observed for larger HAs (215 and 741 kDa). The 67 kDa HA had a conjugation efficiency intermediate to the smaller and larger HA.

3.3. Lung Distribution and Clearance of HA–IR Dye Conjugates

HA–IR dye conjugates were used in a pilot study to help determine HA residence in the lung and to guide the selection of optimal time points and duration for the radiolabeled HA studies. Each mouse received 1 mg/mL of HA–IR instilled at the top of the trachea. Tissue samples were imaged at 1, 8, and 24 h. Each polymer was detected in all five lobes of the lungs for all three time points (Figure 2). The distribution of HA with different molecular weights appeared to be relatively equivalent throughout all the lung lobes for both lungs.

The highest molecular weight HA exhibited the highest level of fluorescence at 1 h (Figure 3). As HA molecular weight decreased from 741 kDa to 30 kDa, fluorescence in the lungs correspondingly decreased. The 215 and 741 kDa HA had significantly higher levels at 1 h compared to the other three HA molecular weights while the two smallest HAs, 7 kDa and 30 kDa, were not significantly different at 1 h. All five molecular weights of HA had minimal fluorescence at 8 and 24 h, suggesting that subsequent studies should last no longer than 8 h.

3.3.1. Radiolabeled HA Physiochemical Properties—HA molecular weight was determined experimentally to compare HA as received to the HA conjugated with tyrosine, which was used for the radiolabeled HA biodistribution studies.[24] The molecular weights of HA molecules measured using SEC were at least 2-fold (and up to 10-fold) higher than the molecular weights reported for these stock HAs (Table 1). Tyrosine conjugation resulted in an apparent decrease in molecular weight compared to stock HA for all five molecular weights though the differences were relatively minor for 7, 30, and 67 kDa HA. The tyrosine conjugation efficiency was similar throughout the different molecular weights ranging from 1.6% for the 7 kDa HA to ~2.3% for the next three higher molecular weights (Table 2). Subsequent ^{125}I conjugation was straightforward. The three middle molecular weights of HA (30, 67, and 215 kDa) had similar levels ranging from 83 to 89%. The 7 kDa and 741 kDa had lower levels of ^{125}I conjugation, 32 and 41% respectively (Table 2).

3.3.2. Distribution and Clearance of HA–^{125}I Conjugates—Animals were instilled with different concentrations of radiolabeled HA into the lungs due to viscosity constraints of the test articles. The three lowest molecular weights, 7, 30, and 67 kDa, were instilled at

11 to 12 mg/mL, while the 215 kDa HA was dosed at 2.8 mg/mL and 741 kDa at 1.6 mg/mL (Table 2). The 7, 30, and 67 kDa HAs had minimal viscosity when instilled into the animals, whereas viscosity increased dramatically for the 215 and 741 kDa HAs (Table 1).[56] Viscosity increased ~3-fold between each molecular weight studied and increased 30-fold and 100-fold when comparing 7 kDa to 215 and 741 kDa HA, respectively.

After instillation, high levels of HA were found in the left and right lung lobes and in the GI tract including the stomach and intestine (Figures 4–6 and Supplemental Figure S1). The shape of the lung exposure profiles over time was similar for all HA molecular weights with HA exposure peaking at an early time point and steadily declining thereafter. The magnitude of peak HA exposure to the lungs (1 to 2 h) depended on HA molecular weight (Figure 4). The 7 kDa HA had the lowest peak levels, with 30 and 741 kDa having the next highest, and 67 and 215 kDa HA having the highest levels in the lungs (Figure 4). At 8 h, 7 and 741 kDa HA displayed the most rapid lung clearance with (approximately 75% and 50% of the initial dose cleared, respectively). In contrast, only approximately 20% of the initial dose of 30, 67, and 215 kDa HA that reached the lungs after intratracheal instillation had been cleared by 8 h post dose. It is important to note that the values in Figure 4 are averaged so the total percent of delivered dose is twice those levels.

The GI tract also showed significant levels of HA (Figures 5 and 6) after intratracheal instillation as expected. In the stomach, the exposure profiles of 7, 30, and 67 kDa HA peaked at 1 h and decreased over the remaining time of the study, while 215 and 741 kDa HA peaked at 2 h. At the final time point of the study (8 h), all five molecular weights of HA had similar levels in the stomach with approximately 5% of the initial dose remaining. In the intestines, the profiles mirror the stomach but all five molecular weights peaked at 1 h and had approximately 5% of the initial dose remaining at 8 h.

The distribution and pharmacokinetics of HA were assessed for other organs and tissues (Figure 7). The liver and trachea had HA exposure levels of approximately 1 to 4% of the initial dose, while the heart, spleen, kidneys, and bladder contained only a fraction of a percent of the initial dose. Interestingly, the level of HA in the trachea increased over time for all five molecular weights of HA.

Pharmacokinetic parameters were modeled to determine HA exposure and elimination from organs. HA half-life in the lungs and heart generally increased as HA molecular weight increased (Table 3). As HA molecular weight increased from 7 kDa to 215 kDa, half-life increased in the lungs from 2 h to nearly 15 h, but 741 kDa HA had a short half-life (4.9–7.5 h) in the lungs. Half-lives for the other organs appeared relatively consistent across the various HA molecular weights with the exception of the heart (Table 3). The heart half-life increased from 3.7 to 13.5 h as HA molecular weight increased from 7 kDa HA to 741 kDa HA; however, this calculation was based on less than 1% exposure to the heart tissue.

Area under the curve (AUC)[31] trended similarly to the half-lives calculated for the different HA molecular weights (Table 4). AUCs increased as HA molecular weight increased from 7 to 215 kDa HA, but sharply declined for the 741 kDa HA. The low levels of HA exposure to the heart increased as HA molecular weight increased. Other organs exhibited relatively

consistent AUC values across the HA sizes studied. Organ clearance rates were also calculated to describe how quickly the HA was removed from each tissue based on the extent of exposure of HA in each organ over time (Supplemental Table S1). Clearance rates from the lungs decreased as molecular weight increased from 7 to 215 kDa HA, but the 741 kDa HA had a higher clearance rate from the lungs, which follows earlier elimination half-life trends. The heart clearance rate decreased as molecular weight increased, while the majority of the other organs (liver, stomach, intestine, and kidney) had clearance rates that remained relatively consistent as HA molecular weight increased.

4. DISCUSSION

4.1. Characterization of HA and Labeled HA

HA is known to self-associate, a phenomenon which can occur within the same polymer chain or between different HA polymer chains. As a result, HA has the potential to form secondary structures within only 6 monomer units, while tertiary structures can occur in polymers as small as 16 monomer units.[11,61,62] These interactions can yield high viscosity solutions, especially for high molecular weight HA (>100 kDa). Careful selection of high salinity mobile phases and dilution of samples is required to accurately analyze HA, since many analytical techniques for polymers are based on mobility. For example, DLS measurements assume diffusion of a sphere as calculated using the Stokes–Einstein equation; however, changes in viscosity can result in differences in apparent size.[63,64] DLS measurements reported here corresponded relatively well to theoretical predictions of radii for the different HA molecular weights studied. Molecular weight approximations of HA were higher than expected, but the trends followed as predicted from the stock HAs.

Similarly, HA self-association has the potential to block reactive sites when attempting to conjugate functional groups. The conjugation of tyrosine was quite low (~2%), while IR dye conjugation was much higher, suggesting poor reactivity of the tyrosine more than simple steric hindrance. ^{125}I labeling, on the other hand, was quite efficient with conjugation exceeding 50%, which is typical for HA. In addition, ^{125}I labeling maintained HA molecular weight by avoiding reducing agents such as cyanoborohydride, which can degrade HA into smaller fragments as was observed with carbon-14 or tritium.[24,42] Overall, conjugated HAs provided a wide range of molecular weights and hydrodynamic sizes for quantitatively tracking pulmonary deposition and subsequent distribution.

4.2. Pulmonary HA Studies

HA has been administered via several routes in a number of species to determine its local and systemic transport. Most reports have focused on higher molecular weight HA (≥500 kDa) delivered by intravenous, subcutaneous, or intrasynovial injections since these are used in dermal fillers and viscosupplements.[5,7,39] Recently, HA has been incorporated into pulmonary formulations primarily as an excipient to increase dose tolerability when treating inflammation. Nebulized HA (300 to 500 kDa) has been administered to mice at a concentration of ~3 mg/mL with a total dose of 6 mg to treat lung inflammation. HA treatment controlled inflammation by decreasing multiple cytokines including TNF-α and macrophage inflammatory protein-2.[25] Nebulized HA formulations employing molecular

weights of 300 to 500 kDa (0.1% HA) were given twice daily in humans to treat lung inflammation. [25–29] Inclusion of HA in the nebulized formulation decreased the length of hospital stay, increased tolerability of the formulation, and reduced lung secretions.[25–29] HA has also been incorporated into drug delivery strategies to improve formulation characteristics. For example, pulmonary administration utilizing spray dried 2 MDa HA with recombinant insulin was administered to beagle dogs. HA increased the mean residence time and terminal half-life of insulin in the lung.[41]

Pulmonary administration includes the possibility of swallowing a portion of the dose directly or after mucociliary clearance. The fate of HA after swallowing is therefore an important consideration when interpreting studies reported here. Oral administration has been studied in both rats (100 kDa to 1 MDa HA) and dogs (1 MDa HA).[20,21] A majority of the orally administered HA remained in the GI tract. There was minimal difference between molecular weights of HA in terms of distribution with only a slightly higher percentage observed in the stomach at 1 h with 0.1 MDa HA compared to 1 MDa. One study found that less than 10% and typically 1–3% of the administered dose of HA was absorbed and detected in peripheral tissues.[21] A second study reported slightly contradictory results where only a trace amount (less than 0.1% of the dose/gram) of orally dosed HA entered systemic circulation.[20] Both studies showed that the vast majority of HA was eliminated in the feces (~85–95%). [20,21]

4.3. Distribution and Clearance of Labeled HA

A pilot study was first conducted using HA–IR to determine the approximate length of time HA may persist in lung tissue. After instillation, HA–IR appeared to disperse evenly throughout all lung lobes for all HA molecular weights. The instilled solutions exhibited similar low viscosities, which may have facilitated exposure throughout the lungs due to gravity since mice were suspended in an upright position. Previous studies indicated that the HA–IR conjugate is unlikely to dissociate especially in innocuous conditions in the lungs.[8,34,65,66] The highest molecular weight HAs showed significantly higher lung exposure at 1 h when compared to the two smallest sizes of HA. The low lung exposures suggested that 7 and 30 kDa HA were rapidly cleared from the lung, since all animals received similar doses. Molecules of this size have been reported to be absorbed from the lung into systemic circulation.[32,33,67] These pronounced differences compelled a more quantitative investigation of rapid HA elimination from mouse lungs (<8 h) and subsequent biodistribution.

Intratracheal instillation of HA–^{125}I showed that the vast majority of HA persisted in the lungs with some clear differences between different HA molecular weights. The 7 kDa HA may have exhibited increased mucociliary clearance due to its high mobility and low viscosity, but data from the trachea suggests that this is unlikely. Increased clearance for the 7 kDa HA may be attributed to increased systemic absorption as seen with the pharmacokinetic data (Tables 3,4, and S1), which led to the highest elimination constant as well as possible urinary elimination since it is below the renal clearance cutoff of 25 kDa. As seen with the increasing half-life in the heart, there is more systemic absorption attributed clearance with the lower molecular weights of HA, which decreases as molecular weight

increases. Data (profiles from the trachea in Figure 7) showed that mucociliary clearance was relatively constant for 7, 30, 67, and 215 kDa HA, suggesting that the increased persistence of larger molecular weights of HA could potentially contribute to the decreased systemic absorption by passive diffusion. As passive diffusion decreases with increasing molecular weight, macrophage uptake might be expected to contribute a larger percentage of clearance for the larger polymers as macrophages typically removed larger particles. The increased persistence seen with 67 and 215 kDa HA might therefore reflect saturation of macrophage and mucociliary clearance and minimal clearance via absorptive clearance mechanisms. Conversely, the very high molecular weight and high viscosity of 741 kDa may have led to retention in upper airways, thus shortening the distance to clear this material into the oropharyngeal cavity, thereby accelerating clearance when compared to the 67 and 215 kDa HA.

HA exposure to the GI tract likely resulted from a portion of the administered dose being swallowed or from mucociliary clearance out of the lungs followed by ingestion. Previous studies have shown limited absorption of 100 kDa to 1 MDa HA and little absorption after oral administration with the majority of the dose being excreted in the feces or remaining in the GI tract.[20,21] The similar level of all molecular weights of HA in the intestines compared to the stomach suggested gastric emptying over the first hour, which could be detected in future studies by more frequent sampling at early time points. The profile shapes can be explained by continuous mucociliary clearance and swallowing followed by gastric emptying contributing to this extended GI accumulation period. The trachea levels increased over time for all 5 molecular weight HAs, which agrees with mucociliary clearance bringing HA from the lungs continuously, independent of polymer size.[68,69] The gastric emptying and GI motility were also expected to be independent of molecular weight for the entirety of the GI tract, thus providing a likely explanation for the similar profiles.[70,71]

The distribution and pharmacokinetics of radiolabeled HA were assessed for other organs and tissues (Figure 7). The heart had very low levels for all molecular weights, which is in agreement with the short circulation half-life reported for HA. The liver specifically eliminates endogenous HA, therefore rapid and continuous elimination of HA from the circulation by the liver was expected.[13,15,19] The kidneys had lower levels than the liver but more than the heart, spleen, and bladder, suggesting that urinary excretion may be another potential route for eliminating the small amounts of HA absorbed systemically from the lung.[12–14] HA content in the bladder tissue was low at all time points. The radiolabel content of urine was not assessed due to difficulties in consistently collecting all urine excreted by mice without the use of metabolic caging.

The 67 kDa and 215 kDa HA may provide the optimal range of size and viscosity for persisting in the lungs (Table 1). For comparison, studies with dendrimers have shown that lung persistence incrementally increased as molecular weight increased from 11 to 22 to 78 kDa.[59] By increasing the size of the dendrimer, researchers observed decreased degradation with lower systemic exposure and greater lung retention.[27] These observations correlate with the molecular weight observed for HAs that persisted in the lungs. The relative hydrophobic character of HA may also contribute to differences in lung persistence, until HA solution viscosity limited penetration of the instilled dose. The hydrophobicity of HA increases as

molecular weight increases.[63] Increasing hydrophobicity of drug delivery systems is known to increase clearance by macrophages, which patrol the deep lung.[72] The 67 and 215 kDa HA may exhibit the most favorable balance of hydrophobicity and hydrophilicity to escape significant macrophage clearance and reduce mucociliary clearance along with mucus gel. In contrast, the 741 kDa HA may not have enough hydrophilic character to facilitate dissolution in the lung fluid thus promoting accelerated mucociliary clearance. The increase in size from 67 to 215 kDa could also be advantageous for facilitating dissolution into lung fluid, while remaining small enough to avoid macrophage clearance.

4.4. Lymphatic Transport of HA

HA naturally clears from tissue spaces through the lymphatics and has been studied as a vehicle to passively target drug delivery to lymph nodes. Properties including molecular size, hydrophobicity,[57] charge,[58] and injection site[58] affect lymphatic delivery.[57,60] Because of its molecular properties, HA has the potential to traffic to the lymphatics after instillation into the lungs. Here, HA exposure to lymph nodes associated with the upper thoracic cavity was also assessed. Brachial nodes draining the upper thoracic exhibited higher levels of HA compared to axillary nodes, but the HA levels were only ~0.02% of the initial delivered dose (Supplemental Figure S2). There was no difference between right or left lymph node, which correlated to the similar HA levels observed in both the right and left lungs (Supplemental Figure S1). It is noteworthy that 741 kDa HA content in the spleen was higher than that of other molecular weights of HA. HA can bind to CD44 on immune cells, which could explain the increase. The 741 kDa HA may have shown this as many endogenous HA lymphatic clearance mechanisms are for molecular weights larger than 100 kDa.

Previous studies have investigated the transport of high molecular weights of HA (4.3 to 5.5 MDA) as well as a low molecular weight HA (150 kDa) injected directly into lymph vessels of sheep.[35] A large percentage of HA was degraded (between 48 and 75%) with a clearance rate of 43 μg/h, and no HA ≥ 1 MDa was detected in the blood. HA of various sizes (6.4 to 697 kDa HA) has also been injected into the footpads of mice, and the fluorescently labeled HA molecules were tracked.[54] This study determined that HA ~30 to 50 nm in size (~75 kDa HA) had the optimal size to access the lymphatics.[54] Similarly, 67 and 215 kDa HA were found here to persist in lung tissues, suggesting that lymphatic transport may be augmented by persistence of the HA in tissues supplying the regional lymphatic network.

5. CONCLUSION

HA is a natural biopolymer that has been used in dermal fillers and viscosupplements, and more recently as an anti-inflammatory therapy and delivery vehicle for therapeutics. The lungs of several animal models and even humans have been treated with HA, thus compelling an improved understanding of HA exposure and elimination from lungs. HAs of different molecular weights (7, 30, 67, 215, and 741 kDa HA) were instilled into the lungs of mice and tracked using a fluorescent label or a radiolabel. HA was predominately found in the lungs and the GI tract. The trachea and liver exhibited the next highest HA exposure, but these tissues had significantly lower amounts of HA compared to the lungs and the GI tract. In the lungs, 7 kDa HA exhibited the lowest exposure levels, and 30 and 741 kDa HA

showed modest exposure, while 67 and 215 kDa exhibited the highest. Pharmacokinetic modeling indicated that 67 kDa and 215 kDa HA offered the longest half-life in the lungs. Also, HA was detectable in mouse lymph nodes draining the lungs and in spleens, suggesting that radiolabeled HA may be interesting to study in animal models of inflammatory lung diseases. Understanding the biodistribution and pharmacokinetics of different molecular weights of HA delivered to the lungs may enable approaches to increase lung persistence or to preferentially access selected tissue compartments to increase therapeutic efficacy.

Supplementary Material

Refer to Web version on PubMed Central for supplementary material.

Acknowledgments

Lab funding was provided by the University of Kansas Department of Pharmaceutical Chemistry, National Institutes of Health (R01 CA173292), and the Dynamic Aspects of Chemical Biology Training Grant (T32 GM08545). We would like to thank the Drug Delivery Disposition and Dynamics center at Monash Institute of Pharmaceutical Sciences for use of facilities, the Macromolecule and Vaccine Stabilization Lab (University of Kansas) for equipment use, the University of Kansas Radiation Safety group for their guidance, and the University of Kansas Animal Care Unit for transport and housing of the animals. L.M.K. was supported by an NHMRC Career Development Fellowship.

REFERENCES

1. Kuo, JW. Practical Aspects of Hyaluronan Based Medical Products. Boca Raton, FL: CRC Press; 2006.
2. Schanté CE, Zuber G, Herlin C, Vandamme TF. Chemical modifications of hyaluronic acid for the synthesis of derivatives for a broad range of biomedical applications. Carbohydr. Polym. 2011; 85(3):469–489.
3. Sugiura G, Kühn H, Sauter M, Haberkorn U, Mier W. Radiolabeling Strategies for Tumor-Targeting Proteinaceous Drugs. Molecules. 2014; 19(2):2135–2165. [PubMed: 24552984]
4. Motokawa K, Hahn SK, Nakamura T, Miyamoto H, Shimoboji T. Selectively crosslinked hyaluronic acid hydrogels for sustained release formulation of erythropoietin. J. Biomed. Mater. Res., Part A. 2006; 78(3):459–465.
5. Fakhari, Amir. Biomedical Application of Hyaluronic Acid Nanoparticles. Dissertation from University of Kansas; 2012.
6. Allison DD, Grande-Allen KJ. Hyaluronan: a powerful tissue engineering tool. Tissue Eng. 2006; 12(8):2131–2140. [PubMed: 16968154]
7. Necas J, Bartosikova L, Brauner P, Kolar J. Hyaluronic Acid (Hyaluronan): a Review. Vet. Med. (Prague, Czech Repub.). 2008; 53(8):397–411.
8. Jiang D, Liang J, Noble PW. Hyaluronan as an Immune Regulator in Human Diseases. Physiol. Rev. 2011; 91(1):221–264. [PubMed: 21248167]
9. Jiang D, Liang J, Noble PW. Hyaluronan in Tissue Injury and Repair. Annu. Rev. Cell Dev. Biol. 2007; 23:435–461. [PubMed: 17506690]
10. Laurent TC, Laurent UBG, Fraser JRE. The Structure and Function of Hyaluronan: an Overview. Immunol. Cell Biol. 1996; 74(2):A1–A7. [PubMed: 8724014]
11. Laurent T, Fraser JR. Hyaluronan. FASEB. 1992; 6(7):2397–2404.
12. Laurent TC. Biochemistry of Hyaluronan. Acta Oto-Laryngol. 1987; 104(s442):7–24.
13. Hascall VC. Hyaluronan, a common thread. Glycoconjugate J. 2000; 17(7–9):607–616.
14. Brown MB, Jones SA. Hyaluronic acid: a unique topical vehicle for the localized delivery of drugs to the skin. J. Eur. Acad. Dermatol. Venereol. 2005; 19(3):308–318. [PubMed: 15857456]

15. Burdick JA, Prestwich GD. Hyaluronic Acid Hydrogels for Biomedical Applications. Adv. Mater. 2011; 23(12):H41–H56. [PubMed: 21394792]
16. Reed R, Laurent U, King S, Fraser J, Laurent T. Effect of Increased Interstitial Fluid Flux on Fractional Catabolic rate of High Molecular Weight [3H]Hyaluronan Injected in Rabbit Skin. Acta Physiol. Scand. 1996; 156(2):93–98. [PubMed: 8868264]
17. Reed R, Laurent U. Removal rate of [3H] hyaluronan injected subcutaneously in rabbits. Am. J. Physiol. 1990; 259(2 Part 2):H532–H535. [PubMed: 2386226]
18. Laurent UB, Dahl LB, Reed RK. Catabolism of Hyaluronan in Rabbit Skin Takes Place Locally, in Lymph Nodes and Liver. Exp. Physiol. 1991; 76(5):695–703. [PubMed: 1742011]
19. Allen S, Fraser R, Laurent U, Reed R, Laurent T. Turnover of hyaluronan in the rabbit pleural space. J. Appl. Physiol. 1992; 73(4):1457–1460. [PubMed: 1447091]
20. Laznicek M, Laznickova A, Cozikova D, Velebny V. Preclinical pharmacokinetics of radiolabeled hyaluronan. Pharmacol. Rep. 2012; 64(2):428–437. [PubMed: 22661195]
21. Balogh L, Polyak A, Mathe D, Kiraly R, Thuroczy J, Terez M, Janoki G, Ting Y, Bucci L, Schauss A. Absorption, Uptake and Tissue Affinity of High-Molecular-Weight Hyaluronan after Oral Administration in Rats and Dogs. J. Agric. Food Chem. 2008; 56(22):10582–10593. [PubMed: 18959406]
22. Fraser R, Laurent T, Engstrom-Laurent A, Laurent U. Elimination of Hyaluronic Acid From the Blood Stream in the Human. Clin. Exp. Pharmacol. Physiol. 1984; 11(1):17–25. [PubMed: 6713733]
23. Fraser R, Laurent T, Pertoft H, Baxter E. Plasma clearance, tissue distribution and metabolism of hyaluronic acid injected intravenously in the rabbit. Biochem. J. 1981; 200(2):415–424. [PubMed: 7340841]
24. Gustafson S, Bjorkman T, Westlin J-E. Labelling of high molecular weight hyaluronan with 1251-tyrosine: studies in vitro and in vivo in the rat. Glycoconjugate J. 1994; 11(6):608–613.
25. Gavina M, Luciani A, Villella VR, Esposito S, Ferrari E, Bressani I, Casale A, Bruscia EM, Maiuri L, Raia V. Nebulized Hyaluronan Ameliorates Lung Inflammation in Cystic Fibrosis Mice. Pediatr Pulmonol. 2013; 48(8):761–771. [PubMed: 22825912]
26. Buonpensiero P, De Gregorio F, Sepe A, Di Pasqua A, Ferri P, Siano M, Terlizzi V, Raia V. Hyaluronic Acid Improves “Pleasantness”, and Tolerability of Nebulized Hypertonic Saline in a Cohort of Patients with Cystic Fibrosis. Adv. Ther. 2010; 27(11):870–878. [PubMed: 20953746]
27. Casale M, Sabatino L, Frari V, Mazzola F, Dell’Aquila R, Baptista P, Mladina R, Salvinelli F. The potential role of hyaluronan in minimizing symptoms and preventing exacerbations of chronic rhinosinusitis. Am. J. Rhinol. Allergy. 2014; 28(4):345–348. [PubMed: 25197922]
28. Furnari ML, Termini L, Traverso G, Barrale S, Bonaccorso MR, Damiani G, Piparo CL, Collura M. Nebulized hypertonic saline containing hyaluronic acid improves tolerability in patients with cystic fibrosis and lung disease compared with nebulized hypertonic saline alone: a prospective, randomized, double-blind, controlled study. Ther. Adv. Respir. Dis. 2012; 6(6):315–322. [PubMed: 22968159]
29. Nenna R, Papoff P, Moretti C, De Angelis D, Battaglia M, Papasso S, Bernabucci M, Cangiano G, Petrarca L, Salvadei S, Nicolai A, Ferrara M, Bonci E, Midulla F. Seven Percent Hypertonic Saline —0.1% Hyaluronic Acid in Infants With Mild-To-Moderate Bronchiolitis. Pediatr Pulmonol. 2014; 49(9):919–925. [PubMed: 24574431]
30. Smyth, HDC.; Hickey, AJ. Controlled Pulmonary Drug Delivery. New York, NY: Springer Publishing; 2011.
31. Winkler J, Hochhaus G, Derendorf H. How the Lung Handles Drugs Pharmacokinetics and Pharmacodynamics of Inhaled Corticosteroids. Proc. Am. Thorac. Soc. 2004; 1:356–363. [PubMed: 16113458]
32. Patton J, Byron P. Inhaling medicines: delivering drugs to the body through the lungs. Nat. Rev. Drug Discovery. 2007; 6(1):67–74. [PubMed: 17195033]
33. Patton J, Fishburn CS, Weers J. G The Lungs as a Portal of Entry for Systemic Drug Delivery. Proc. Am. Thorac. Soc. 2004; 1:338–344. [PubMed: 16113455]
34. Bailey MM, Berkland CJ. Nanoparticle Formulations in Pulmonary Drug Delivery. Med. Res. Rev. 2009; 29(1):196–212. [PubMed: 18958847]

35. Fraser J, Kimpton W, Laurent T, Cahill R, Vakakis N. Uptake and degradation of hyaluronan in lymphatic tissue. Biochem. J. 1988; 256(1):153–158. [PubMed: 3223897]
36. Reed R, Laurent T, Taylor A. Hyaluronan in prenodal lymph from skin: changes with lymph flow. Am. J. Physiol. Heart Circ. Physiol. 1990; 259(4):1097–1100.
37. Kim Y, Lee Y-S, Hahn J-H, Choe J, Kwon HJ, Ro JY, Jeoung D. Hyaluronic acid targets CD44 and inhibits FcRI signaling involving PKC, Rac1, ROS, and MAPK to exert anti-allergic effect. Mol. Immunol. 2008; 45(9):2537–2547. [PubMed: 18289679]
38. Casalino-Matsuda SM, Monzon ME, Day AJ, Forteza RM. Hyaluronan Fragments/CD44 Mediate Oxidative Stress-Induced MUC5B Up-Regulation in Airway Epithelium. Am. J. Respir. Cell Mol. Biol. 2009; 40(3):277–285. [PubMed: 18757307]
39. Garg, HG.; Hales, CA. Chemistry and Biology of Hyaluronan. Atanta, GA: Elsevier Science; 2004.
40. Smedsrod B, Pertoft H, Eriksson S, Fraser R, Laurent T. Studies in vitro on the uptake and degradation of sodium hyaluronate in rat liver endothelial cells. Biochem. J. 1984; 223(3):617–626. [PubMed: 6508733]
41. Surendrakumar K, Martyn GP, Hodgers ECM, Jansen M, Blair J. A Sustained release of insulin from sodium hyaluronate based dry powder formulations after pulmonary delivery to beagle dogs. J.Controlled Release. 2003; 91(3):385–394.
42. Orlando P, de Sanctis G, Giordano C, Valle G, la Bua R, Ghidoni R. Tritium Labeled Hyaluronic Acid Derivative. J. Labelled Compd. Radiopharm. 1985; 22(9):961–969.
43. Orlando P, Binaglia L, De Feo A, Orlando M, Trenta R, Trevisi R. An Improved Method for Hyaluronic Acid Radioiodination. J. Labelled Compd. Radiopharm. 1995; 36(9):855–859.
44. Cozikova D, Laznickova A, Hermannova M, Svanovsky E, Palek L, Buffa R, Sedova P, Koppova R, Petrik M, Smejkalova D, Laznicek M, Velebny V. Preparation and the kinetic stability of hyaluronan radiolabeled with 111In. J. Pharm. Biomed. Anal. 2010; 52(4):517–524. [PubMed: 20189740]
45. Oh EJ, Park K, Kim KS, Kim J, Yang J-A, Kong J-H, Lee MY, Hoffman AS, Hahn S. K Target specific and long-acting delivery of protein, peptide, and nucleotide therapeutics using hyaluronic acid derivatives. J. Controlled Release. 2010; 141(1):2–12.
46. Möller L, Krause A, Bartsch I, Kirschning A, Witte F, Drager G. Preparation and In Vivo Imaging of Lucifer Yellow Tagged Hydrogels. Macromol. Symp. 2011; 309/310(1):222–228.
47. Kadi S, Cui D, Bayma E, Boudou T, Nicolas C, Glinel K, Picart C, Auzely-Velty R. Alkylamino Hydrazide Derivatives of Hyaluronic Acid:Synthesis, Characterization in Semidilute Aqueous Solutions, and Assembly into Thin Multilayer Films. Biomacromolecules. 2009; 10(10):2875–2884. [PubMed: 19769354]
48. Ossipov D, Kootala S, Yi Z, Yang X, Hilborn J. Orthogonal Chemoselective Assembly of Hyaluronic Acid Networks and Nanogels for Drug Delivery. Macromolecules. 2013; 46(10):4105–4113.
49. Prestwich G, Marecak D, Marecek JF, Vercruysse KP, Ziebell M. R Controlled chemical modification of hyaluronic acid: synthesis, applications, and biodegradation of hydrazide derivatives. J. Controlled Release. 1998; 53(1–3):93–103.
50. Rydergren, S. Chemical Modifications of Hyaluronan using DMTMM-Activated Amidation. Thesis from Uppsala University; 2013.
51. D'Este M, Eglin D, Alini M. A systematic analysis of DMTMM vs EDC/NHS for ligation of amines to Hyaluronan in water. Carbohydr. Polym. 2014; 108:239–246. [PubMed: 24751270]
52. Farkas P, Cízová A, Bekesová S, Bystricky S. Comparison of EDC and DMTMM efficiency in glycoconjugate preparation. Int. J. Biol. Macromol. 2013; 60:325–327. [PubMed: 23791662]
53. Rayamajhi M, Redente EF, Condon TV, Mercedes G-J, Riches DWH, Lenz LL. Non-surgical intratracheal instillation of mice with analysis of lungs and lung draining lymph nodes by flow cytometry. J. Visualized Exp. 2011; 51:2702.
54. Bagby TR, Cai S, Duan S, Thati S, Ares DJ, Forrest L. Impact of Molecular Weight on Lymphatic Drainage of a Biopolymer-Based Imaging Agent. Pharmaceutics. 2012; 4(2):276–295. [PubMed: 24300232]

55. Takahashi R, Kubota K, Kawada M, Okamoto A. Effect of Molecular Weight Distribution on the Solution Properties of Sodium Hyaluronate in 0.2M NaCl Solution. Biopolymers. 1999; 50(1):87–98.
56. Mendichi R, Soltés L, Giacometti Schieroni A. Evaluation of radius of gyration and intrinsic viscosity molar mass dependence and stiffness of hyaluronan. Biomacromolecules. 2003; 4(6): 1805–1810. [PubMed: 14606912]
57. Prokop, Ales. Intracellular Delivery—Fundamentals and Applications. New York, NY: Springer Publishing; 2011.
58. Bagby TR, Duan S, Cai S, Yang Q, Thati S, Berkland C, Ares DJ, Laird Forrest M. Lymphatic trafficking kinetics and near-infrared imaging using star polymer architectures with controlled anionic character. Eur. J. Pharm. Sci. 2012; 47(1):287–294. [PubMed: 22546180]
59. Ryan G, Kaminskas LM, Kelly BD, Owen DJ, McIntosh MP, Porter CJH. Pulmonary Administration of PEGylated Polylysine Dendrimers: Absorption from the Lung versus Retention within the Lung Is Highly Size-Dependent. Mol. Pharmaceutics. 2013; 10(8):2986–2995.
60. Kaminskas LM, Porter CJH. Targeting the lymphatics using dendritic polymers (dendrimers). Adv. Drug Delivery Rev. 2011; 63(10–11):890–900.
61. Scott J, Cummings C, Brass A, Chen Y. Secondary and tertiary structures of hyaluronan in aqueous solution, investigated by rotary shadowing-electron microscopy and computer simulation. Biochem. J. 1991; 274(3):699–705. [PubMed: 2012600]
62. Heatley F, Scott JE. A water molecule participates in the secondary structure of hyaluronan. Biochem. J. 1988; 254(2):489–493. [PubMed: 2845953]
63. Size matters: Rh versus Rg. Malvern Corporate Meet the Experts Press Release. 2012 Nov 15.
64. Zwanzig R, Harrison AK. Modifications of the Stokes-Einstein formula. J. Chem. Phys. 1985; 83(11):5861–5862.
65. Mori M, Yamaguchi M, Sumitomo S, Takai Y. Hyaluronan-Based Biomaterials in Tissue Engineering. Acta Histochem. Cytochem. 2004; 37(1):1–5.
66. Vindigni V, Cortivo R, Iacobellis L, Abatangelo G, Zavan B. Hyaluronan Benzyl Ester as a Scaffold for Tissue Engineering. Int. J. Mol. Sci. 2009; 10(7):2972–2985. [PubMed: 19742179]
67. Patton J, Platz RM. Routes of Delivery: Case Studies: Pulmonary delivery of peptides and proteins for systemic action. Adv. Drug Delivery Rev. 1992; 8(2–3):179–196.
68. Grubb BR, Jones JH, Boucher RC. Mucociliary transport determined by in vivo microdialysis in the airways of normal and CF mice. Am. J. Physiol. Lung Cell Mol. Physiol. 2004; 286(3):L588–L595. [PubMed: 14633516]
69. Foster WM, Walters DM, Longphre M, Macri K, Miller L. Methodology for the measurement of mucociliary function in the mouse by scintigraphy. J. Appl. Physiol. 2001; 90(3):1111–1118. [PubMed: 11181627]
70. Padmanabhan P, Grosse J, Asad ABMA, Radda GK, Golay X. Gastrointestinal transit measurements in mice with 99mTc-DTPA-labeled activated charcoal using NanoSPECT-CT. EJNMMI Res. 2013; 3(60):1–8. [PubMed: 23281702]
71. Schwarz R, Kaspar, Künnecke S. Gastrointestinal transit times in mice and humans measured with 27Al and 19F nuclear magnetic resonance. Magn. Reson. Med. 2002; 48(2):255–261. [PubMed: 12210933]
72. Loira-Pastoriza C, Todoroff J, Vanbever R. Delivery strategies for sustained drug release in the lungs. Adv. Drug Delivery Rev. 2014; 75:81–91.

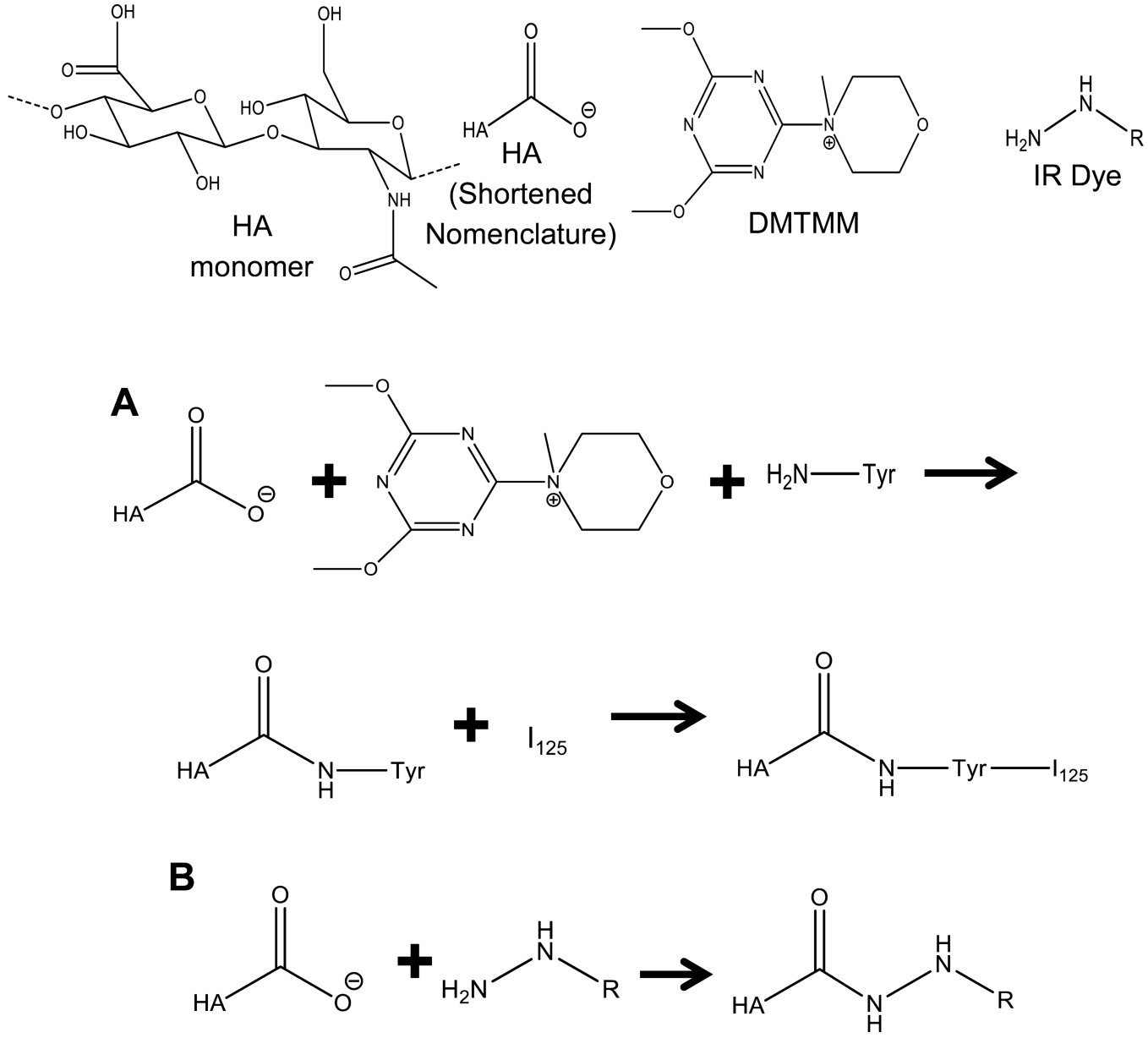

Figure 1.

Depiction of full HA monomer unit, abbreviated HA, DMTMM molecule, and IR dye as a hydrazine group. (A) Chemical reaction of HA with DMTMM and tyrosine for tyrosine conjugation followed by addition of ^{125}I for radiolabeled HA. (B) Hydrazine IR dye reaction leading to conjugation on HA.

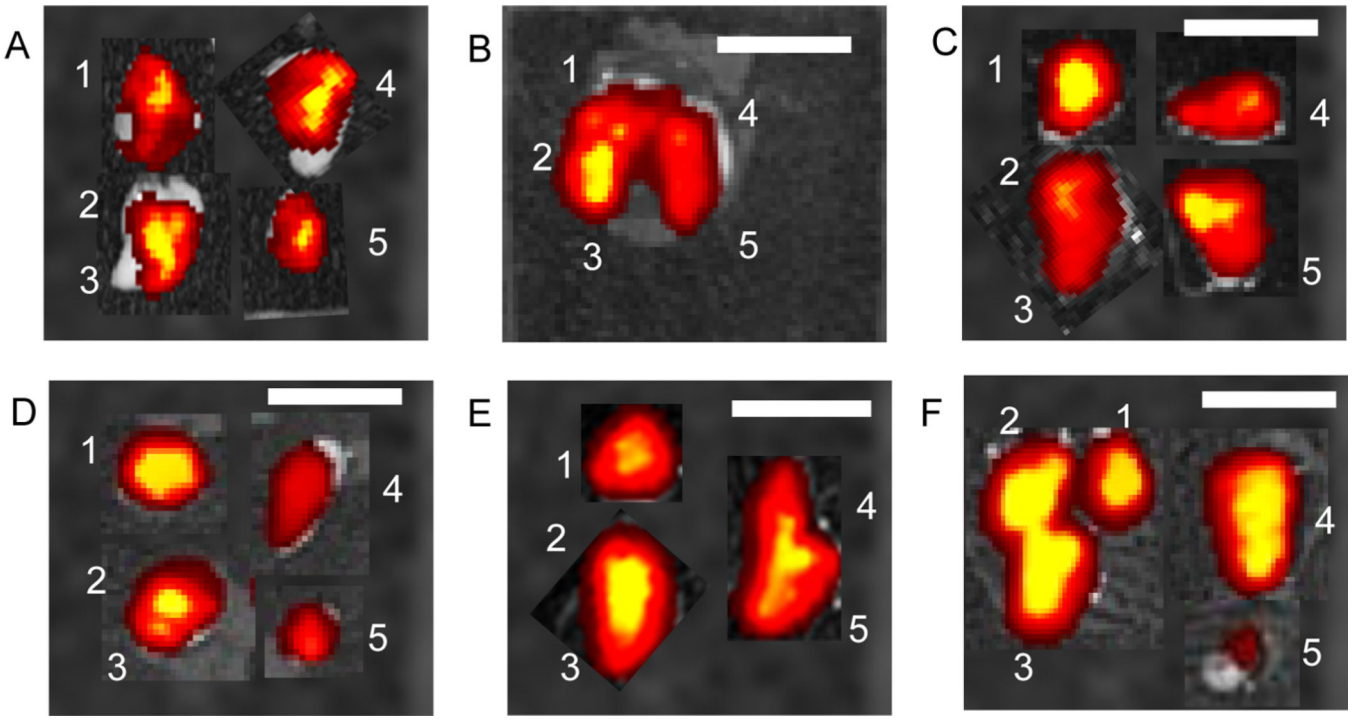

Figure 2.

Fluorescent images of lungs injected with HA-IR showing distribution though out all lung lobes with all five different molecular weights. (A) Lungs injected with 5 μL of 7 kDa HA solution; (B) 7 kDa HA 8 h; (C) 30 kDa HA 8 h; (D) 67 kDa HA 8 h; (E) 215 kDa HA 8 h; (F) 741 kDa 8 h. White scale bar is 1 cm. The white numbers represent lobes of the lungs with 1, 2, and 3 representing mouse anatomical right lung lobes and 4 and 5 representing mouse anatomical left lung lobes.

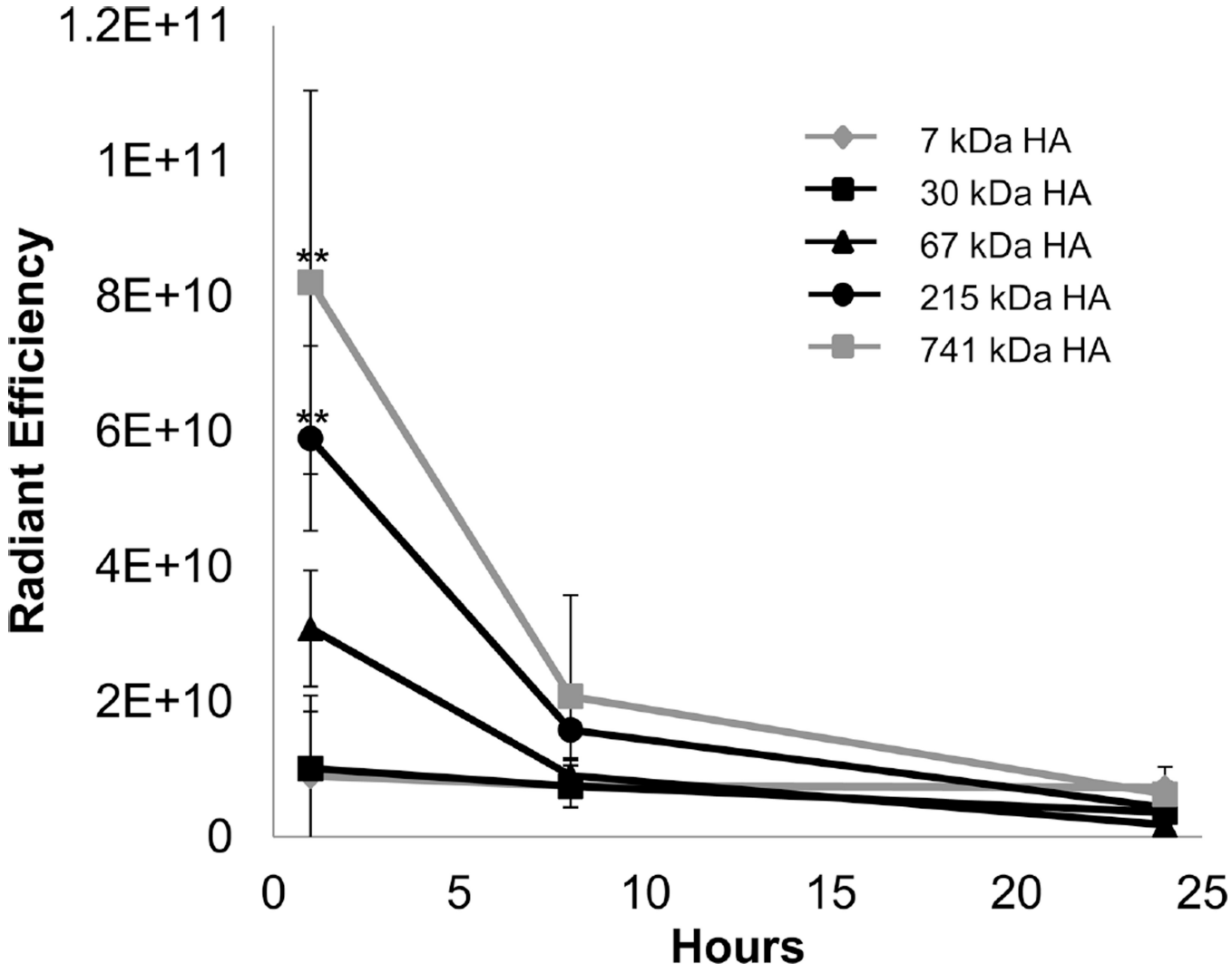

Figure 3.

Analysis of lungs instilled with HA–IR dye. The largest molecular weight of HA had the longest persistence in the lungs which decreased with molecular weight. ** signifies statistical difference from 7, 30, and 67 kDa HA, and each point is the average of at least three animals.

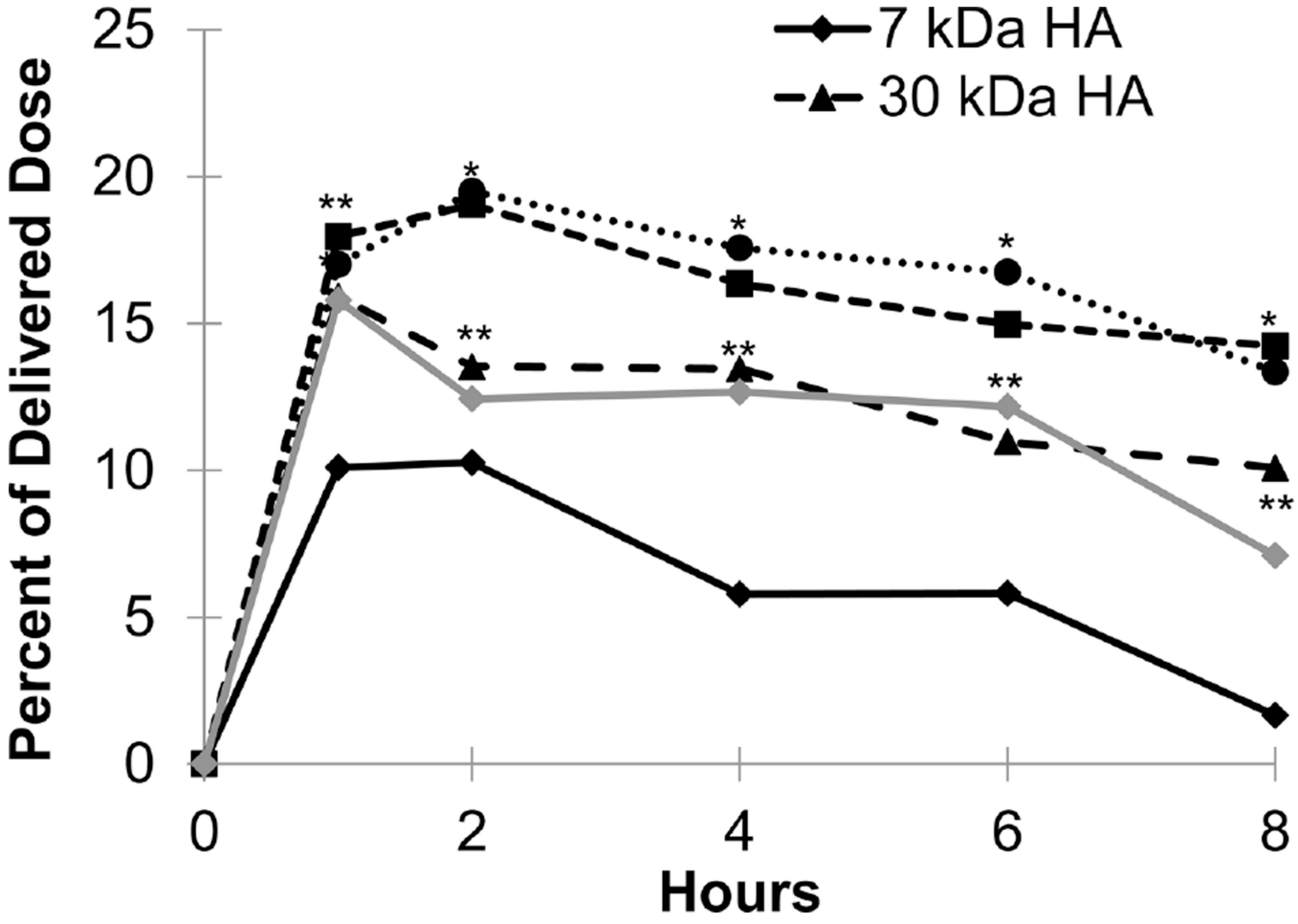

Figure 4.

Exposure levels of HA in the lungs averaged across both right and left lung lobes as a percentage of delivered dose over time for each of the five HA molecular weights. Each point is an average of at least five animals with the error on each point <5% of the measurement. * represents *p* value <0.05 for 67 kDa and 215 kDa HA compared with 7 kDa, 30 kDa, and 741 kDa HA. ** represents p value <0.05 for 30 kDa and 741 kDa HA compared with 7 kDa, 67 kDa, and 215 kDa HA. *** represents *p* value <0.05 for 30 kDa, 67 kDa, 215 kDa, and 741 kDa HA compared with 7 kDa HA.

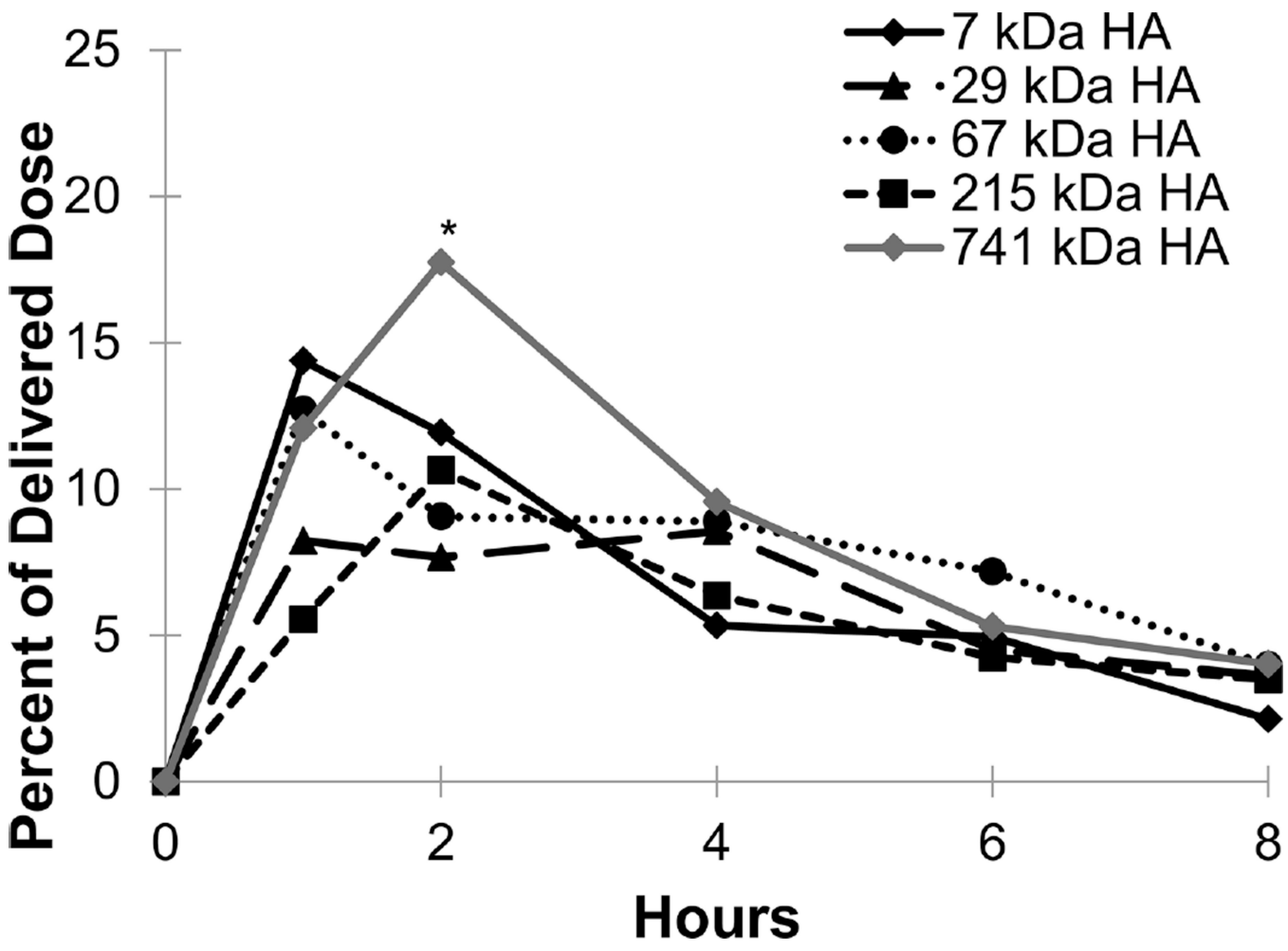

Figure 5.

Exposure levels of HA in the stomach as a percentage of delivered dose over time for each of the five HA molecular weights. Each point is an average of at least five animals with the error on each point <5% of the measurement. * represents p value <0.05 for 741 kDa HA compared with 7 kDa, 30 kDa, 67 kDa, and 215 kDa HA.

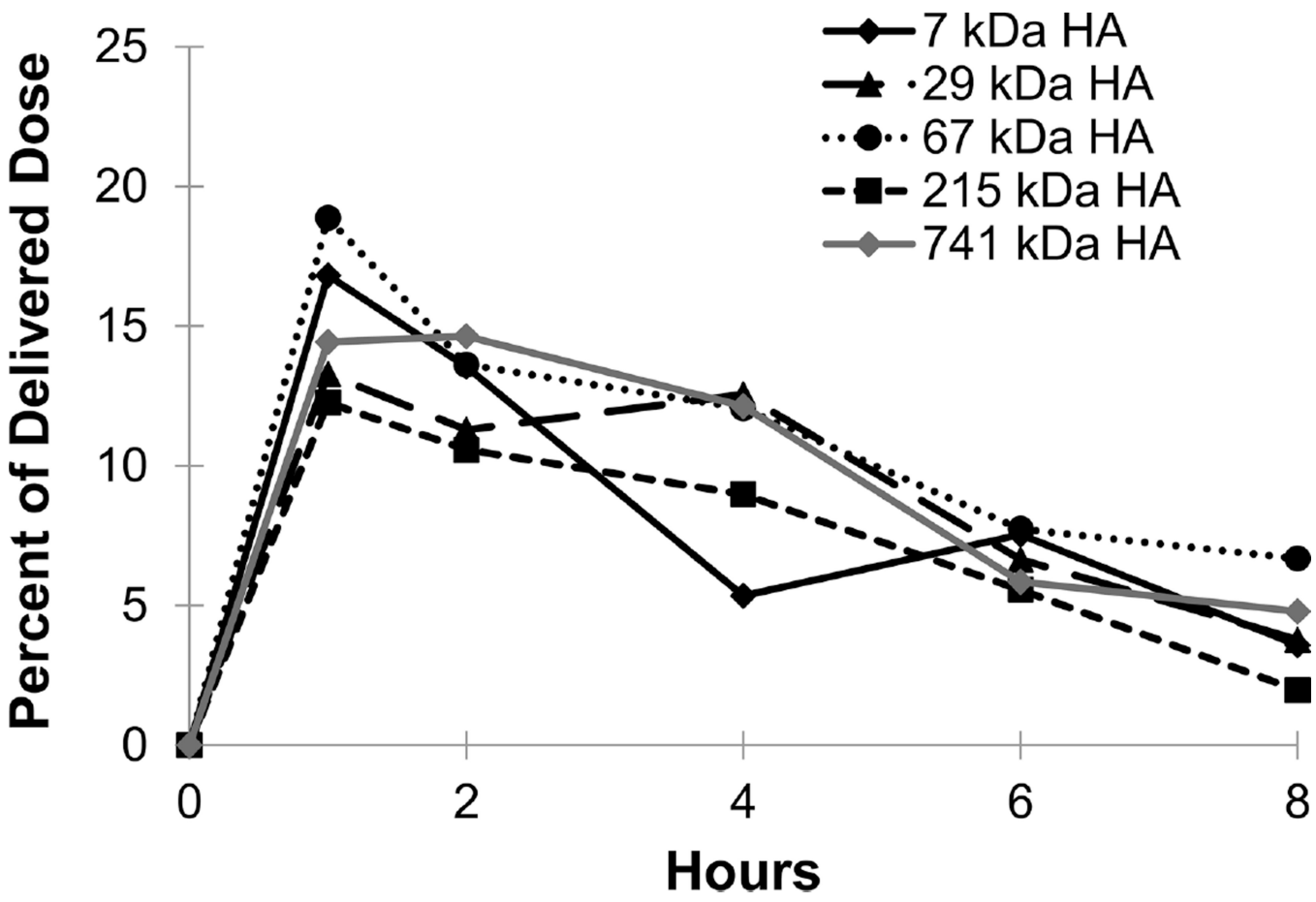

Figure 6.

Exposure levels of HA in the intestine as a percentage of delivered dose over time for each of the five HA molecular weights. Each point is an average of at least five animals with the error on each point <5% of the measurement.

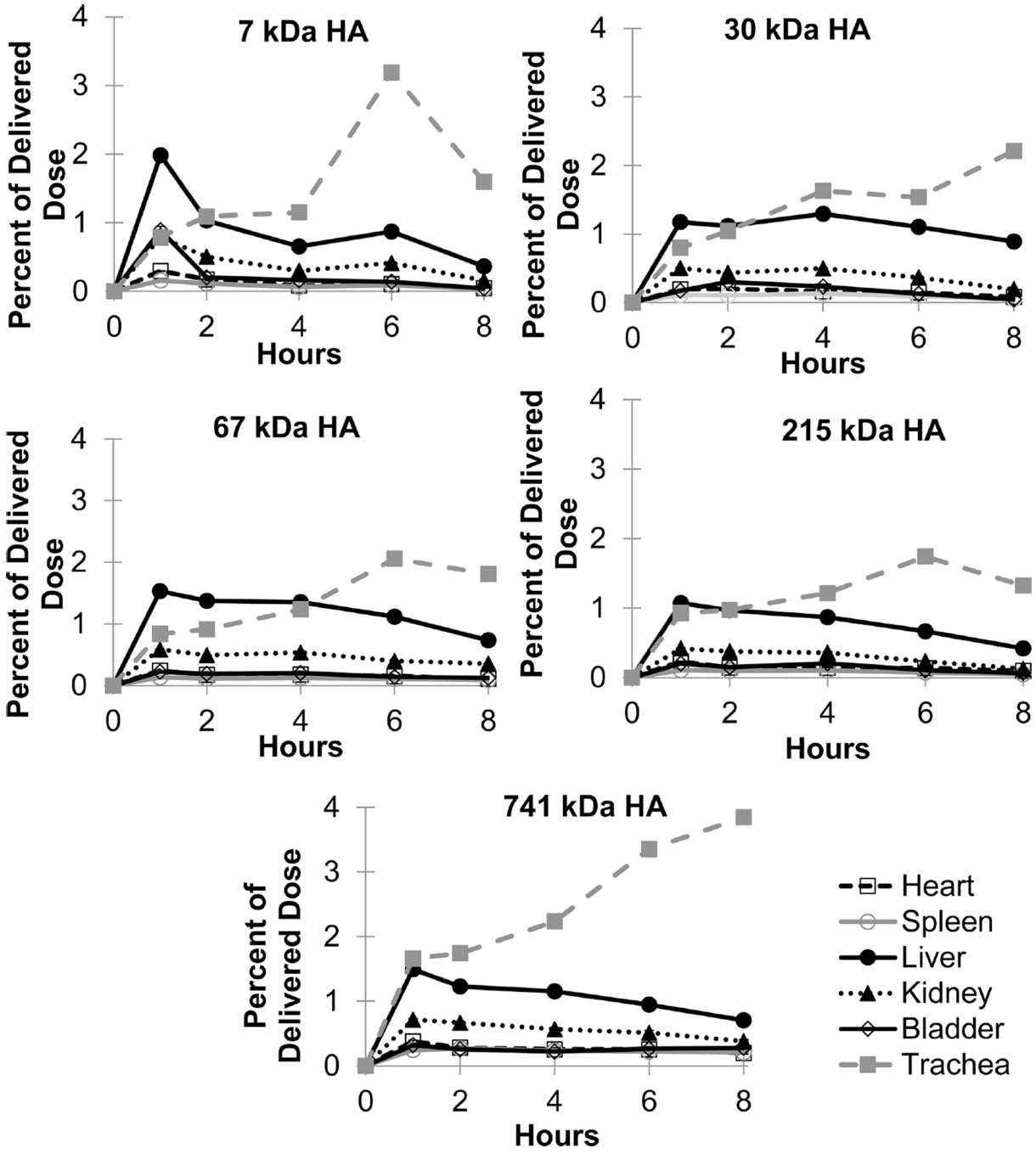

Figure 7.

Exposure levels of HA in the heart, spleen, liver, kidney, bladder, and trachea based on molecular weight with 7 and 29 kDa HA on top, 67 and 215 kDa HA in the middle, and 741 kDa HA on the bottom as a percentage of delivered dose over time for each of the five HA molecular weights. Each point is an average of at least five animals with the error on each point <5% of the measurement.

Table 1

Calculated and Experimental Sizes of Different Molecular Weights of HA

MW (kDa)	calcd radius of gyration (Rg) (nm)	calcd hydrodynamic radius (Rh) (nm)	DLS measurements (nm)	size based on SEC data (kDa)[b]	SEC HA-tyrosine (kDa)[b]	calcd viscosity (dL/g)
7	7.1	3.0	6.1 ± 0.2	14 ± 3	13 ± 2	14.8
30[a]	16.3	7.4	12.2 ± 1.3	68 ± 7	59 ± 4	68.9
67	25.8	12.3	22.1 ± 1.2	155 ± 14	127 ± 9	161.0
215	50.2	25.6	33.3 ± 0.2	557 ± 28	435 ± 18	477.3
741	101.6	53.9	55.0 ± 0.7	1646 ± 51	451 ± 25	1250.0

[a]Calculations based on an estimated molecular weight of 30 kDa HA. Lots were 29 kDa and 31 kDa. DLS and SEC data were performed for the 29 kDa HA lot.

[b]Standard deviations were based on running the same samples for three different runs.

Table 2

Conjugation Efficiency of HA in the Different Reactions to IR Dye, Tyrosine, and HA–Tyrosine to ^{125}I

	conjugation efficiency (%)			
MW (kDa)	IR dye	tyrosine	^{125}I	concn of HA in intratracheal instillation soln (mg/mL)
7	72.3	1.6	32.7	12.1
30[a]	69.7	2.4	83.3	11.1
67	50.5	2.3	83.6	11.5
215	38.3	2.3	88.9	2.8
741	36.6	NA	41.1	1.6

[a]Lots were 29 kDa and 31 kDa. Conjugation efficiency of IR dye was performed on the 31 kDa HA lot, while conjugation efficiency of tyrosine, conjugation efficiency of I^{125}, and concentration of HA in intratracheal instillation solution data were performed for the 29 kDa HA lot. NA represents not available.

Table 3

Organ Half-Life in Hours for Each Tissue Based on Molecular Weight

	lung lobes								
MW (kDa)	**right**	**left**	**heart**	**spleen**	**liver**	**stomach**	**intestine**	**kidney**	**bladder**
7	2.5	2.1	3.7	4.0	4.9	2.7	3.8	4.3	2.8
30[a]	9.8	11.0	3.9	2.8	7.4	3.2	2.3	2.9	1.7
67	9.5	10.8	5.5	9.0	4.5	3.5	5.4	6.7	5.7
215	29.8	14.7	7.4	3.4	3.8	4.6	1.8	2.6	2.4
741	4.9	7.5	13.5	17.8	5.6	3.2	3.0	7.8	ND

[a]HA molecular weight of 30 kDa was composed of lots of 29 and 31 kDa. ND represents not determined.

Table 4

Area under the Curve (AUC) in h·μg/mL for Each Tissue Based on Molecular Weight

	lung lobes								
MW (kDa)	**right**	**left**	**heart**	**spleen**	**liver**	**stomach**	**intestine**	**kidney**	**bladder**
7	328.2	344.4	7.42	5.15	57.3	380.1	518.5	24.7	12.12
30[a]	1370.1	1363	9.11	5.31	100.2	367.8	471.9	21.6	8.38
67	1913.3	1797.0	12.09	11.59	80.8	471.7	788.0	40.0	13.31
215	4471.2	2305.3	12.19	5.01	47.6	398.8	370.1	15.9	7.67
741	917.3	850.2	33.95	40.33	80.6	526.0	566.0	49.2	ND

[a]HA molecular weight of 30 kDa was composed of lots of 29 and 31 kDa. ND represents not determined.